Gap junction and amino acid import in somatic cells promote germ cell growth

Caroline Vachias[1], Camille Tourlonias[1], Louis Grelée[1], Nathalie Gueguen[1], Yoan Renaud[1], Parvathy Venugopal[1], Graziella Richard[1], Pierre Pouchin[1], Émilie Brasset[1], Vincent Mirouse[1*]

1) Université Clermont Auvergne, Institute of Genetics, Reproduction and Development (iGReD), - UMR CNRS 6293 - INSERM U1103, Faculté de Médecine, 28 Place Henri-Dunant, 63000 Clermont-Ferrand, France

*contact: vincent.mirouse@uca.fr

Key words

Drosophila, innexins, germ cells, metabolism, SLC36, P-bodies

Abstract

Gap junctions allow the exchange of small molecules between cells. How this function could be used to promote cell growth is not yet fully understood. During *Drosophila* ovarian follicle development, germ cells, which are surrounded by epithelial somatic cells, undergo massive growth. We found that this growth depends on gap junctions between these cell populations, with a requirement for Innexin4 and Innexin2, in the germ cells and the somatic cells, respectively. Translatomic analyses revealed that somatic cells express enzymes and transporters involved in amino acid metabolism that are absent in germ cells. Among them, we identified an amino acid transporter required for germline growth. Its ectopic expression in the germline can compensate for its absence in somatic cells. Moreover, affecting either gap junctions or amino-acid import in somatic cells induces P-bodies in the germ cells, a feature associated with an arrest of translation. Finally, in somatic cells, innexin2 expression and gap junction assembly are regulated by the insulin receptor/PI3K kinase pathway. Overall, these results support the view that metabolic transfer through gap junction promotes cell growth and illustrate how such a mechanism can be integrated into a developmental programme, coupling growth control by extrinsic systemic signals with the intrinsic coordination between cell populations.

Introduction

Gap junctions are channels between adjacent cells. Each cells harbour a hemichannel made of six subunits, connexins in vertebrates and innexins in other animal phyla where gap junctions are found. These two protein families are very different in terms of primary sequence, but similar in terms of conformation (1-4). Hemichannels can be homomeric or heteromeric in composition and channels can be formed from two identical or different hemichannels, leading to a large range of channel combinations with different regulations or solute specificities. Gap junctions generally assemble in plaques that contain many channels and each channel allows the direct communication, and thus molecular flows, between the cytoplasm of two cells. However, due to the channel size and conformation, only passive transfer of small molecules and ions, up to approximatively 1KDa, including second messengers (e.g. inositol triphosphate and calcium) is allowed. Gap junction proteins also participate in other cellular mechanisms, such as cell migration (5,6). Moreover, many molecules that can diffuse through gap junctions are linked to energetic metabolism (e.g. glucose and pyruvate) and to anabolic metabolism (e.g. amino acids). However, despite many studies on these metabolite flows, their functional relevance has been elusive.

Such metabolite exchanges could promote cell growth. Available genetic data suggest that the growth of mammalian oocytes could be an illustration of such a mechanism. Indeed, mutation of connexin 37 (*Cx37*) in germ cells or of *Cx43* in somatic granulosa cells, which surround and are in contact with the oocyte, strongly impairs oocyte and follicle growth (7,8). Moreover, amino acid import and pyruvate production are more efficient in follicle cells, and granulosa cells are required for an effective uptake of some amino acids, including alanine and proline, by the oocyte (9-12). These data suggest a potential metabolic flow towards the oocyte via the gap junctions. Nonetheless, it is not known: i) to which extent this putative transfer of metabolites contributes to explain gap junction impact on oocyte growth; and ii) whether such mechanism is coupled with follicle cell growth and more generally, is integrated in the genetic programme controlling follicle development.

A major feature of oocytes is their large size throughout animal evolution, despite important variation among species (13,14). Their size prefigures the early embryo size and their content will determine the early embryo development success rate and quality (15,16). Hence, oocyte growth is an essential step that requires robust underlying mechanisms (17,18). Oocyte development and growth usually occur in ovarian follicles where germ cells are surrounded by follicle cells (i.e. somatic epithelial cells). *Drosophila* oogenesis takes place in a structure called ovariole, in which follicles continuously arise and develop from the anterior to the posterior end. Each ovary is subdivided in about 16 ovarioles (Fig. 1A). Follicles bud from a structure called the germarium that contains germ cells and somatic stem cells. Follicle development is divided in 14 morphological stages during which the oocyte volume increases 1000 times in about 3 days before being fertilized and laid (19). At stage 1, a follicle contains a germline cyst of 16

interconnected cells: 15 nurse cells that will grow by endoreplication and 1 oocyte at the posterior end, blocked in early meiosis. Each germline cyst is encapsulated by the follicular epithelium that is initially composed of about 30 cells. These cells proliferate giving 800 cells at stage 6 and then they undergo endoreplication (20). Both germ cell growth and follicle cell growth are cell autonomously sensitive to the usual growth systemic signals, such as the Insulin Receptor/Phosphatidylinositol 3 Kinase (InR/PI3K) and Target of Rapamycin (TOR) pathways (18,21-23). These pathways affect also non-cell autonomously the growth of the adjacent tissue in both direction: the soma influences germline growth and *vice versa* (18,22-25). The most striking illustration of this reciprocal coordination is observed when *Pten*, a InR/PI3K repressor, is mutated in follicle somatic cells. The faster growth of these somatic cells induces the faster growth of the surrounded wild-type germ cells. Regulation of somatic cell growth by germline growth involves the Hippo pathway and its modulation by tension induced on the epithelium due to the germline cyst volume increase (26). However, it is not known how the follicle somatic cells control germ cell growth.

Here, we tested the hypothesis of an evolutionary conservation of gap junction function between germ cells and follicle cells to regulate *Drosophila* female germ cell growth and explored the underlying mechanism. Several reports indicate that gap junctions are present during fly oogenesis. In gem cells, innexin 4 (Inx4) forms plaques at the contact with follicle cells (27-29). Several innexins, including Inx2, are expressed in follicle cells and partially colocalize with or are juxtaposed to Inx4 (28,29). Inx4 is required for germ cell survival before follicle formation, and Inx2 is involved in the germline cyst encapsulation by follicle cells during follicle budding (27,30,31). Inx2 and Inx4 are also required for morphogenetic events during oogenesis. such as the stretching of anterior follicle cells and the migration of border cells during stage 9 (6,29). Moreover, Inx4 and Inx2 form gap junctions in the testis where they are required at different steps of sperm development (27,32,33).

We found that Inx4/Inx2 gap junctions are required for female germline growth once follicles are formed. Moreover, follicle cells specifically express genes involved in amino acid biology, and amino acid import in follicle cells is necessary for germline growth. This germline growth control by somatic follicle cells is linked to the formation of processing bodies (P-bodies) and can be partially bypassed by the direct expression of an amino acid transporter in the germline. Moreover, gap junction assembly is controlled by the InR/PI3K pathway, thus connecting growth coordination between these two cell types with systemic growth control.

102 **Results**

103 **Inx2 and Inx4 form gap junctions at the soma-germline interface that are required for**
104 **germline growth**

105 As gap junctions are required for oocyte growth in mammals, we asked whether they could play
106 a similar role in *Drosophila* oogenesis (7,8). Therefore, first, we characterized the gap junction
107 composition and profile in somatic and germ cells, focusing on stages 1 to 8 when follicle
108 development is globally limited to growth without major morphogenetic changes. As previously
109 described (27-29), we detected Inx2 and Inx4 forming plaques at the interface between germ and
110 somatic cells. Inx2 also formed plaques on the lateral domain of follicle cells (Fig. 1B-E). Inx2
111 expression and plaque size tended to increase as follicles developed (Fig. S1A). The cytoplasmic
112 signal localization suggested that Inx2 and Inx4 were mainly expressed in the soma and germline,
113 respectively. Accordingly, *Inx2* knock-down (*Inx2* RNAi) induction in somatic clones led to the cell-
114 autonomous loss of Inx2 staining, whereas induction of *Inx4* knock-down (*Inx4* RNAi) in the
115 germline led to the loss of Inx4 staining (Fig. 1F,G). Notably, we did not detect Inx4 at the contact
116 of *Inx2* RNAi follicle cells, confirming published results (Fig. 1F''') (29). Similarly, when *Inx4* was
117 knocked down in germline cysts, we did not detect Inx2 plaques at the germline contact, although
118 Inx2 protein expression was increased in follicle cells (Fig. 1G'''). This last observation could
119 suggest a feedback mechanism between gap junction formation and Inx2 expression. Moreover,
120 the loss of *Inx2* in the germline or *Inx4* in the soma did not induce visible defects (Fig. S1B,C).
121 Altogether, these data clearly established the presence of gap junction plaques composed of Inx4
122 in the germline and of Inx2 in follicle cells, and the Inx4-Inx2 interdependence for plaque assembly.
123 We then tested whether these gap junctions influenced germline growth by generating large *Inx2*
124 mutant clones. In such conditions, we observed follicles that were smaller than the younger one
125 at their anterior, a phenomenon never observed in the wild-type ovarioles. The quantification of
126 the ratio between the volumes of the defective growth follicle and the follicle at its anterior
127 confirmed these observations (Fig. 1H,I). We observed this phenotype with three different alleles,
128 and only when all (or almost) epithelial cells of a follicle harboured the mutated *Inx2* while the
129 anterior one was wild-type or contained a smaller percentage of mutant cells. Similar cases with
130 control clones had no visible effect (Fig. S1D). Because it is known that germline and somatic
131 growth influence each other, we aimed to determine whether *Inx2* effect on germline growth was
132 due to a cell-autonomous effect on somatic growth (22,24,34). We analysed follicle cell growth in
133 smaller clones that do not induce germline defect to avoid feedback between tissues. In such
134 mutant cells we did not observe any difference in cell size and in the proportion of cells in S phase
135 (EDU-positive) between these populations, indicating that Inx2 did not influence somatic growth
136 in a cell autonomous manner (Fig. 1J-K). This suggests that gap junctions are specifically required
137 for germline growth. We could not confirm this hypothesis using germline null *Inx4* mutant clones
138 because in these mutant germline cysts development is blocked very early in the germanium (27).

139 Therefore, we generated *Inx4* RNAi clones in the germline, directly detected by the absence of
140 Inx4 expression (Fig. 1G). *Inx4* RNAi cysts were not larger than the younger wild-type follicle,
141 indicating defective germline growth (Fig. 1G,L). Altogether, these data indicate that Inx2 and Inx4
142 form homomeric and heterotypic gap junctions between somatic and germ cells that are required
143 for germ cell growth.
144
145 **Genes implicated in amino acid metabolism are enriched in somatic follicular cells**
146 Gap junction requirement for germ cell growth supports a model in which metabolites diffuse from
147 follicle cells to germ cells. However, the direct identification of such metabolites is technically
148 challenging. We hypothesized that if follicle cells produce or import metabolites not present in the
149 germline, we might identify enzymes or transporters that are involved in this process and are
150 expressed only in follicle cells. To this aim, we performed translating ribosome affinity purification
151 (TRAP), an approach that allows identifying the tissue-specific translatome. We used
152 *nanos:Gal4VP16* and *trafficjam:Gal4* drivers to express a GFP-tagged ribosomal protein
153 (UASp:RPL10a-GFP) specifically in the germline and in somatic cells, respectively (Fig. 2A). Then,
154 we immunoprecipitated the GFP-tagged polysomes and isolated and sequenced the associated
155 mRNAs under translation. Our biological replicates were highly reproducible (Table S1 and Fig.
156 S2). To extract genes with a specific or strongly enriched somatic expression we used a fold-
157 change of 5 between soma and germline as cut-off that gave a list of 811 genes (Fig. 2B). We then
158 selected genes involved in small molecule metabolic processes, reducing the list to 52 genes. The
159 whole ecdysone synthesis pathway (six genes), which is exclusively active in follicle cells, was
160 enriched in follicle cells, thus validating our TRAP approach (35). Moreover, six genes encoding
161 enzymes involved in amino acid biosynthesis were specifically expressed in follicle cells (Fig. 2B).
162 By analysing this GO class, we found that 29 enzymes were expressed in both cell types, but none
163 was germline-specific (Fig. 2C). Similarly, among the 60 amino acid transporters encoded by the
164 fly genome, 21 were expressed in both tissues, 12 were specifically expressed in the soma, and
165 none in the germline alone (Fig. 2B,D). These data indicated that among the genes specifically
166 expressed in follicle cells there is a strong bias for genes involved in amino acid synthesis or
167 import. Given the importance of these metabolites for growth, they are good candidates to be
168 transferred through gap junctions.
169
170 **Amino acid import in follicle cells is required for germline growth**

171 Then, we performed a reverse genetic screen by inducing the silencing (RNAi) of the genes
172 involved in amino acid synthesis or transport identified by TRAP in follicle cells and then looking
173 for ovary growth defects. For each amino acid many redundancies may occur between anabolic
174 pathways or transporters that may preclude the observation of clear phenotypes. However, the

175 knock-down of one of the 18 tested genes reproductively induced an ovary growth defect in
176 independent RNAi lines (Fig. 3B-C). This gene, *CG43693*, was uncharacterized in *Drosophila* but
177 belongs to the SLC36 family of amino acid transporters, and was especially close to mammalian
178 SLC36A1 and SLC36A4 that are involved in non-polar amino acids transport as proline, alanine
179 or tryptophan {Boll 2002; Metzner 2006; Pillai 2011

180 We confirmed by RNA-FISH that *CG43693* was specifically expressed in follicle cells and checked
181 for its effective knock-down by RNAi in the somatic lineage (Figs 3D-E and S3A). Moreover, we
182 detected *CG43693* mRNA in all follicle cells and at all stages of oogenesis, and its expression
183 progressively increased with the stage (Fig. 3D). A role in importing amino acids from the
184 haemolymph would require a cell membrane localization, while some amino acid transporters are
185 specific to some intracellular vesicular compartments. Therefore, to determine CG43693 protein
186 localization, we generated a GFP knock-in with the MiMIC system to insert in-frame an EGFP-
187 encoding exon (36). This insertion was in the non-conserved N-terminal part common to five of
188 the seven described *CG43693* isoforms. Importantly, it tags isoforms RA and RB that were
189 expressed in follicle cells according to our TRAP mRNA sequence data. The line C*G43693-GFP*
190 was homozygous viable and fertile without visible phenotype. Moreover, ovary size was normal
191 when C*G43693-GFP* was in trans with a deficiency covering the gene, indicating that the insertion
192 did not affect protein function (Fig S3B). We observed a strong GFP signal that tended to increase
193 throughout oogenesis in follicle cells, as previously observed for the mRNA, but no signal in the
194 germline (Fig. 3D,F). The GFP decorates the whole cortex of follicle cells (Fig. 3G). Thus, both
195 CG43693 tissue distribution and subcellular localization were in agreement with the hypothesis
196 that it is implicated in the import of amino acids to promote follicle growth.
197 We then tested whether CG43693 was required for follicle growth. The Minos element insertion
198 (*CG43693*^{MI101960}) used for the GFP knock-in initially contains an exon with STOP codons in
199 different frames. As it is located in the protein N-terminus, it should induce null mutation of the
200 affected isoforms, which include the ones expressed in follicle cells. This allele was sublethal when
201 homozygous or in trans with a deficiency covering the gene. In both cases, the ovaries of these
202 flies were strongly atrophied, fitting with a role for this gene in follicle growth (Fig. S3B). Moreover,
203 Replacing the STOP codon-containing exon with the GFP exon suppressed ovary growth defect.
204 We generated mutant clones in the follicular epithelium. Analysis of small clones that did not cover
205 the whole epithelium did not show any difference in cell size and proliferation, suggesting that
206 follicle cell growth was not affected (Fig. 3J,K). Conversely, when the whole epithelium of a follicle
207 was mutated, such follicles were smaller (or of the same size) than the younger ones, while control
208 clones did not show the same defect (Figs 3H,I and S3C). As this growth defect led to tiny and
209 round follicles, we called this gene *cochonnet (coch)* after the nickname of the small wood ball
210 used with larger metal boules for pétanque, a traditional game in the South of France. Importantly,

211 these experiments indicated that *coch* expression in somatic follicle cells was required for
212 germline growth.
213
214 **Genetic evidence of a metabolic transfer between soma and germline cells**
215 Our results support a model in which amino acids imported in follicle cells diffuses through gap
216 junctions to sustain germline growth. In this case, germline expression of *coch* should rescue
217 genetic conditions in which it is absent in somatic follicle cells. Importantly, it is known that the
218 follicular epithelium is permeable at least until stage 8, and thus that metabolites from the
219 haemolymph can directly reach oocyte surface (37). To test this hypothesis, we combined the
220 UAS/Gal4 system with the QUAS/QF system (38). We generated a MatTub:QF driver and a
221 QUASp promoter, inspired by the UASp promoter, for proper expression in the germline (39). A
222 Q*UASp:GFP* transgene driven by MatTub:QF was expressed in the germline at all stages, starting
223 slightly earlier than what described for MatTub:Gal4Vp16, indicating that both driver and QUASp
224 promoter were functional (Fig. S4). Expression of the *QUASp:coch* transgene in the germline with
225 the same driver (*MatTub>coch*) had a slight negative effect on ovary size (Fig. 4A-C,F). However,
226 when it was combined with somatic knock-down of *coch* (*tj>cochRNAi),* it rescued the effect of
227 the latter on ovary size (Fig. 4A,D-F). These genetic data demonstrated that the requirement of
228 *coch* expression in follicular cells for germline growth can be compensated by its germline
229 expression, suggesting a direct metabolic exchange between these cell types.
230
231 **Blocking gap junctions or amino acid import induces processing bodies.**
232 Previous studies indicated that somatic growth impairment affects germ cell development (18,22-
233 24). Moreover, the mRNA binding protein Me31B, which is typically concentrated where the
234 anterior-posterior axis determinants localize in the oocyte, becomes enriched in large cytoplasmic
235 structures in the germline when somatic growth is impaired (16,40). These condensates are
236 reminiscent of P-bodies and stress granules observed upon various stresses, including amino
237 acid deprivation (41). In follicles, their formation can be induced by reducing protein availability in
238 fly food and are more easily seen at stage 9 in Me31B-GFP-expressing follicles (40) (Fig. 5A,B).
239 Therefore, we set up a semi-automated method for their quantification by measuring the
240 fluorescence fraction found in condensates in stage 9 nurse cells (Fig. 5C). P-body formation is
241 associated with translation arrest usually induced by inhibitory phosphorylation of the eukaryotic
242 translation initiation factor 2 subunit alpha (eIF2α) on serine 51 (S51) (41). Overexpression in the
243 germline of a transgene mimicking this phosphorylated form (eIF2α-S51D), but not wild-type
244 eIF2α, strongly induced P-body formation, although we did not quantify them because these
245 follicles never reached stage 9 (Fig. 5D,E). Importantly, eIF2α-S51D overexpression was sufficient
246 to completely block germline growth, suggesting a direct link between P-body formation and
247 growth control (Fig. 5E). As P-bodies potentially repress germline growth, we tested whether the

248 absence of gap junctions between germ cells and follicle cells or defective amino acid import in
249 the follicle cells could induce their formation. We knocked down *Inx2* and *coch* in follicle cells
250 using *tj:Gal4* in the presence of Me31B-GFP. Constitutive *Inx2* RNAi in the somatic lineage
251 completely blocked oogenesis and precluded the observation of stages 8-9. Therefore, we added
252 a constitutive *Gal80*^{ts} transgene to allow expression of the RNAi construct only during a short
253 period of time at the permissive temperature (14 hours, at 30°C). *Coch* and *Inx2* knock-down
254 strongly induced the formation of P-bodies, suggesting that the observed growth limitation was
255 linked to their formation and the subsequent arrest of translation (Fig 5F-I).
256 Formation of P-bodies or stress granules following amino acid deprivation can occur
257 independently or dependently of eIF2α S51 phosphorylation. In the first case, which is not the
258 most frequently described, it is associated with the repression of the TOR pathway (42). However,
259 induction of *Tor* RNAi in the germline does not induce P-body formation, excluding this possibility
260 (16). In the second case, eIF2α is phosphorylated by GCN2 that acts as an indirect sensor of
261 amino acid availability. We generated null mutant alleles for *gcn2* that were homozygous viable,
262 as similar alleles described during the course of this project (43-45). Protein deprivation in *gcn2*
263 transheterozygous females still led to P-body formation in the germ cells (Fig. S5A-E). Moreover,
264 an indirect reporter of GCN2 activity and eIF2α–S51 phosphorylation (ATF4-GFP) showed no
265 signal in the germline of wild-type flies, even after protein deprivation (Fig. S5F-G). Lastly, we
266 tested more directly *gcn2* role in the germline when amino acid import in follicle cells is impaired
267 (*tj>cochRNAi*). However, *gcn2* mutant germline clones did not increase the growth rate of wild-
268 type and *coch* RNAi follicles (Fig. S5H,I). These results strongly argued against the implication of
269 GCN2 as a germ cell growth repressor when the availability of the amino acids provided by Coch
270 is reduced.
271 Altogether these data indicate that although the two well-established pathways involved in amino
272 acid sensing do not seem implicated, P-body formation is linked to germ cell growth control by
273 gap junctions and amino acid import in follicle cells.
274
275 **Gap junction assembly links intrinsic growth coordination and systemic control**
276 Published data indicated that InR/PI3K pathway inhibition in follicle cells induces the formation of
277 P-bodies in the germline (16). This result was reproduced by silencing (RNAi) *akt*, an essential
278 actor of this pathway, in follicle cells (Fig. 6A-C). Since somatic activity of the InR/PI3K pathway
279 also strongly influences germline growth, we asked whether there was a link between the InR/PI3K
280 pathway activity in follicle cells and their ability to transfer metabolites to the germline. Coch-GFP
281 expression level and localization were similar in wild-type and in follicle cells with a PI3K gain of
282 function or mutated for *akt,* suggesting no impact on this specific actor of amino acid import in
283 follicle cells (Fig. S6A,B). Conversely, in *akt* mutant cells, Inx2 was almost undetectable (Fig. 6D),
284 whereas Inx2 expression was strongly increased in *Pten* mutant cells and plaques size was

285 increased (Fig. 6E). These data indicated that Inx2 expression is sensitive to InR/PI3K pathway
286 gain and loss of function. We also observed that *Inx2* mRNA level was strongly increased in *Pten*
287 mutant follicle cells, suggesting that the observed effects on protein level and plaque assembly
288 were due *Inx2* upregulation (Fig. 6F). These observations supported a model in which the non-cell
289 autonomous effect of the InR/PI3K pathway from somatic cells to germ cells is mediated by gap
290 junctions. To test this hypothesis, we performed an epistasis experiment. As previously described
291 (18), large *Pten* mutant clones in the follicular epithelium accelerated germline growth in a non-
292 cell autonomous manner (Fig. 6G). This effect was abrogated upon *Inx2* RNAi induction in *Pten*
293 mutant cells (Fig. 6H). Thus, gap junctions are required for germline growth control via InR/PI3K
294 activity in the follicular epithelium. Altogether, our data link the systemic control of somatic cells
295 to the growth coordination between somatic and germline cells via the modulation of gap junction
296 assembly.
297
298

Discussion

In this article we show that gap junctions participate in the control of cell growth, leading to the intuitive proposal that they allow a metabolic flow between cells. In accordance with this hypothesis, we identified an amino acid transporter, *coch*, specifically expressed in follicle cells and required for germline cell growth. Though a flux of amino acids from somatic cells to germ cells cannot be directly visualized, *coch* expression in the germline can partially bypass its silencing in the soma, providing evidence for a functional metabolic exchange between these cell types. Moreover, both defective gap junction or amino-acid import in somatic cells induces P-bodies in the germ cells, a feature associated with an arrest of translation. Thus, collectively, our data lead to a model in which gap junctions allow the transfer from somatic cells to germ cells of metabolites, such as amino acids, that germ cells cannot directly produce or import, thereby promoting germ cell growth through translation control.

Inx2 and Inx4 have various functions during *Drosophila* oogenesis (6,27,29,31). However, our data showing their involvement in germ cell growth can be more easily compared with gap junction role in mammal follicles where Cx37 is expressed in the oocyte and Cx43 in follicle cells (7,8). This indicates that gap junction requirement for oocyte growth is a conserved feature throughout evolution. Gap junctions are present in most animal tissues and can directly connect different cell types, for instance, neurons and glial cells. Therefore, their involvement in growth control might be more general. We found that Inx2 expression and the subsequent formation of plaques were strongly regulated by the InR/PI3K pathway in a cell autonomous manner. This indicates that gap junctions are a permissive prerequisite for germline growth, and it also provides an effective mechanism to link metabolic flow with growth systemic signals and coordinate the growth of the two connected cell populations.

Our results also established that Coch, an amino acid transporter of the SLC36A family, must be expressed in somatic cells for germline growth. Amino acid availability and cell growth control are usually linked by the TOR pathway (46). However, this pathway is unlikely implicated in the mechanism described here. Indeed, first, when germline growth is blocked due to alteration of somatic cell growth upon loss of *akt*, which also regulates gap junction assembly, the TOR pathway is still active in the germline (18). Moreover, overactivation of the TOR pathway in the germline in such conditions does not suppress growth inhibition. Finally, TOR inhibition in the *Drosophila* female germline does not induce P-body formation (16). Therefore, we tested the involvement of the other well-described amino acid sensing pathway that relies on GCN2. Our results also excluded this mechanism to explain P-body formation and growth inhibition in the absence of proline import in somatic cells or of gap junctions. Therefore, more studies are needed to determine the precise mechanism underlying germline growth control. Nevertheless, several arguments suggest that amino acids imported by Coch might just be the tip of the iceberg of the metabolic cooperativity between follicle cells and germ cells. *Inx2* mutant clones have a stronger

337 impact on germline growth than *coch* mutant clones, suggesting that other metabolites from
338 follicle cells also may promote germline growth. Accordingly, our translatome analysis showed
339 that different genes involved in amino acid synthesis or import were specifically expressed in
340 follicle cells, but none in germ cells. The absence of phenotype when these genes were knocked
341 down, except *coch*, could be explained by multiple potential levels of redundancy among
342 synthesis pathways, transporters, and synthesis and import. Nonetheless, detailed analysis of the
343 genes overexpressed in follicle cells compared with germ cells suggest that several amino acids
344 (e.g. proline, tryptophane, valine, tyrosine) could flow from the soma to the germline. Moreover, in
345 the mouse, the alanine transporter SLC38A3 is strongly enriched in granulosa cells that are
346 required for efficient alanine import in the oocyte (11). Thus, altogether these data suggest that
347 gap junction-dependent amino acid flow is not restricted to the amino acids imported via Coch.
348 Besides, glucose intake and pyruvate production are more efficient in granulosa cells, suggesting
349 that follicle cells could provide energetic molecules to the oocyte (12). In line with this observation
350 in mammals, TRAP data indicated that transporter for trehalose (tret1-1), the circulating sugar in
351 insects, was expressed in somatic cells and not in the germline, whereas germline development
352 is highly dependent on sugar and the pentose phosphate pathway (47). Thus, a contribution of
353 energetic metabolism in the soma-germline cooperativity via gap junctions will be an interesting
354 avenue for future investigations.
355 One might ask what is the evolutive advantage of this metabolic cooperativity compared with
356 direct import or synthesis in the germline. Three main hypotheses could be proposed. First,
357 metabolites might not be able to directly reach oocyte membrane due to the presence of the
358 follicular epithelium. However, in follicles from stage 1 to 8, septate junctions are immature, and
359 the epithelium is not impermeable (37). Accordingly, our results showing a rescue of *coch*
360 absence in the soma by its ectopic expression in the germline imply that its solutes can reach the
361 oocyte. Second, female germ cells undergo massive growth and there is a non-linear relation
362 between volume and cell surface increases. Consequently, surface exchange with the extracellular
363 medium might not allow sufficient metabolic import and may require the support of follicle cells.
364 This hypothesis was proposed to explain gap junction requirement for mammal oocyte growth
365 (48). However, in this case, both tissues should be able to import the required metabolites and
366 our data does not support such a model because follicle cells expressed a whole set of anabolic
367 enzymes and transporters that were not expressed in the germline. Alternatively, such a
368 mechanism may provide a protective effect for the germline. It is well established that the cell
369 metabolic activity can induce stress, with for instance, the production of reactive oxygen species
370 (ROS). However, the germline must be protected, especially its DNA content that is transmitted to
371 the embryo. A recent study demonstrated that mammalian oocytes block ROS production by
372 suppressing mitochondrial complex I (49). Thus, a gap junction-mediated metabolic exchange
373 might allow externalizing the stress-generating metabolic activity to follicle cells that will anyway

374 die few days later. Notably, *coch* expression in germ cells had a slight but significant negative
375 impact on ovary size, suggesting that its presence in germ cells is detrimental for follicle
376 development. Although, the exact reason for this deleterious effect is unknown, this observation
377 fits with a model in which externalization of metabolic import and activity could facilitate proper
378 oocyte development. However, Coch is a transporter, and not an enzyme, and thus, the protective
379 effect might not be directly due to amino acid exclusion, but to one of the many possible
380 downstream metabolic activities.
381 Altogether, our data indicate that gap junctions and a metabolic flow are essential for cell growth
382 and that gap junction assembly can be modulated to adjust cell growth rate. Moreover, it shows
383 that amino acids, and potentially other metabolites, are important actors in this mechanism ending
384 with the formation of P-bodies, opening a large field for investigation to obtain a comprehensive
385 view of this metabolic cooperativity.
386

387 **Materials and Methods**

388

389 **Fly genetics and handling**

390 All fly stocks used are detailed in Table S2. The final genotypes, temperature and heat-shock
391 conditions are in Table S3. *gcn2* null alleles were generated by inducing indel mutations using an
392 available gRNA line. Alleles are described in Table S2. Unless specified, flies were kept on a corn
393 meal-based medium with 80 g/L fresh yeast. Protein starvation was performed on grape juice agar
394 plate. Coch-EGFP was obtained by inserting the EGFP-FlAsH-StrepII-TEV-3xFlag cassette in the
395 Minos element insertion MI01960, as previously described (36).

396 **TRAP experiments**

397 Ovaries of 100 females of each genotype (tj>RPL10-GFP or Nos>RPL10-GFP) were dissected on
398 ice. Then, TRAP was performed as described in Bertin et al, 2015. Briefly, after homogenization,
399 ovary extracts were preabsorbed with magnetic beads. Immunoprecipitation was performed with
400 anti-GFP antibodies already coupled with magnetic beads before mRNA extraction. Tissue
401 specificity and enrichment of the extracted mRNAs were checked by RT-qPCR with *GFP*
402 (enrichment), *traffic-jam* (soma specific), *Ago3* and *Aubergine* (germline specific) primers. mRNA
403 libraries were made with the Nugen Ovation 1-16 droso Universal RNA-seq kit according to the
404 manufacturer's instructions. Sequencing was performed by Fasteris. Data were deposited on GEO
405 (GSE230452) and described in Table S1.

406 **Molecular cloning and transgenesis**

407 The *QF* sequence was amplified from the pAttB-QF-sv40 vector and cloned in the vector that
408 contains the alpha4-tubulin promoter (MatTub). The pQUASp vector was constructed from pUAST
409 in which the promoter was replaced by QUAS sites and the minimal P-element promoter was
410 amplified from the pUASp vector. Then, this vector was used to clone *EGFP* or *coch* coding
411 sequence and P-element insertions were generated. *eIF2*α and *eIF2*α*-S51D* coding sequences
412 were cloned in the pUASz vector, and transgenes were inserted at the AttP40 landing site. All
413 vectors and new *Drosophila* lines can be provided upon request.

414 **Immunostaining, FISH, EDU incorporation, imaging and quantitative analyses**

415 Resources and reagents are listed in Table S1. Immunostaining was performed as described in
416 Vachias et al, 2014. Stellaris SM-FISH oligo-probes against *Inx2* and *CG43693/coch* mRNAs were
417 produced by Biosearch Technologies. FISH was performed according to the manufacturer's
418 instruction. Images were acquired on a Zeiss LSM800 confocal microscope or a Zeiss Cell
419 observer spinning disc microscope. P-bodies were quantified using a homemade macro initially
420 designed to quantify basement membrane fibrils (50). Quantifications were done on 5 μm z-stack
421 projections of spinning-disc images acquired with a x20 lens. After manual selection of a ROI
422 corresponding to nurse cells, P-bodies were detected by keeping objects with a minimal size of 5
423 adjacent pixels and a minimal fluorescence intensity of x1.75 of the mean intensity. Then, the total

424 fluorescence contained in these P-bodies was quantified and reported as a fraction of the total
425 fluorescence of the ROI. For EDU incorporation, ovaries were incubated with 10μM EDU in
426 complemented Schneider medium for 15 minutes. After fixation, staining was performed
427 according to the manufacturer's instructions (Kit EDU C10638, Thermo Fisher). Mutant-control
428 follicle volume ratios were calculated after estimating the follicle volume by multiplying their length
429 by their width to the square. Mutant and control follicles in position 2 to 4 of the ovariole starting
430 from the anterior were analyzed. Cell size was automatically determined after cell segmentation
431 using Tissue Analyzer (51). Statistical analyses were performed with Prism. For all experiments,
432 the minimum sample size is indicated in the figure legends. For each experiment, multiple females
433 were dissected. Randomization or blinding was not performed. The sample normality was
434 calculated using the D'Agostino and Pearson normality test. The unpaired *t*-test was used to
435 compare samples with normal distribution (or one-way ANOVA for multiple comparisons), and the
436 unpaired Mann–Whitney test for samples without normal distribution. Figures were prepared using
437 ScientiFig (52).
438
439 **Acknowledgements**
440 We are grateful to G. Junion, P Phelan, G Tanentzapf, H.D. Ryoo for sharing antibodies or fly
441 stocks. We also thank the CLIC facility (Clermont Imagerie Confocale). This research was financed
442 by the French government IDEX-ISITE initiative 16-IDEX-0001 (CAP 20-25).
443
444 **Competing interests**
445 The authors declare no competing or financial interests.
446

447 **Bibliography**

448 1. Bauer R, Löer B, Ostrowski K, Martini J, Weimbs A, Lechner H, Hoch M. Intercellular
449 communication: The drosophila innexin multiprotein family of gap junction proteins. Chemistry &
450 Biology 2005, May;12(5).
451 2. Evans WH. Cell communication across gap junctions: A historical perspective and current
452 developments. Biochem Soc Trans 2015, Jun;43(3).
453 3. Oshima A, Tani K, Fujiyoshi Y. Atomic structure of the innexin-6 gap junction channel
454 determined by cryo-em. Nat Commun 2016;7.
455 4. Skerrett IM, Williams JB. A structural and functional comparison of gap junction channels
456 composed of connexins and innexins. Dev Neurobiol 2017, May;77(5).
457 5. Elias LA, Wang DD, Kriegstein AR. Gap junction adhesion is necessary for radial migration in
458 the neocortex. Nature 2007;448(7156).
459 6. Miao G, Godt D, Montell DJ. Integration of migratory cells into a new site in vivo requires
460 channel-independent functions of innexins on microtubules. Dev Cell 2020;54(4).
461 7. Gittens JE, Kidder GM. Differential contributions of connexin37 and connexin43 to oogenesis
462 revealed in chimeric reaggregated mouse ovaries. J Cell Sci 2005;118(Pt 21).
463 8. Simon AM, Goodenough DA, Li E, Paul DL. Female infertility in mice lacking connexin 37.
464 Nature 1997;385(6616).
465 9. Colonna R, Mangia F. Mechanisms of amino acid uptake in cumulus-enclosed mouse
466 oocytes. Biol Reprod 1983, May;28(4).
467 10. Haghighat N, LJ VW. Developmental change in follicular cell-enhanced amino acid uptake
468 into mouse oocytes that depends on intact gap junctions and transport system gly. The Journal
469 of Experimental Zoology 1990, Jan;253(1).
470 11. Eppig JJ, Pendola FL, Wigglesworth K, Pendola JK. Mouse oocytes regulate metabolic
471 cooperativity between granulosa cells and oocytes: Amino acid transport. Biol Reprod 2005,
472 Aug;73(2).
473 12. Sugiura K, Pendola FL, Eppig JJ. Oocyte control of metabolic cooperativity between oocytes
474 and companion granulosa cells: Energy metabolism. Dev Biol 2005;279(1).
475 13. Doherty CA, Amargant F, Shvartsman SY, Duncan FE, Gavis ER. Bidirectional
476 communication in oogenesis: A dynamic conversation in mice and drosophila. Trends Cell Biol
477 2022, Apr;32(4).
478 14. Church SH, Donoughe S, BAS DM, Extavour CG. Insect egg size and shape evolve with
479 ecology but not developmental rate. Nature 2019, Jul;571(7763).
480 15. Petkova MD, Little SC, Liu F, Gregor T. Maternal origins of developmental reproducibility.
481 Curr Biol 2014, Jun 2;24(11):1283-8.
482 16. Burn KM, Shimada Y, Ayers K, Vemuganti S, Lu F, Hudson AM, Cooley L. Somatic insulin
483 signaling regulates a germline starvation response in drosophila egg chambers. Dev Biol
484 2015;398(2).
485 17. Doherty CA, Diegmiller R, Kapasiawala M, Gavis ER, Shvartsman SY. Coupled oscillators
486 coordinate collective germline growth. Dev Cell 2021;56(6).
487 18. Vachias C, Fritsch C, Pouchin P, Bardot O, Mirouse V. Tight coordination of growth and
488 differentiation between germline and soma provides robustness for drosophila egg
489 development. Cell Rep 2014, Oct 23;9(2):531-41.
490 19. Spradling AC, Bate M, Arias AM. The development of drosophila melanogaster. The
491 Development of Drosophila Melanogaster 1993;1:1-70.
492 20. Chen DY, Crest J, Streichan SJ, Bilder D. Extracellular matrix stiffness cues junctional
493 remodeling for 3D tissue elongation. Nat Commun 2019;10(1).
494 21. Drummond-Barbosa D, Spradling AC. Stem cells and their progeny respond to nutritional
495 changes during drosophila oogenesis. Dev Biol 2001, Mar 1;231(1):265-78.
496 22. LaFever L, Feoktistov A, Hsu HJ, Drummond-Barbosa D. Specific roles of target of
497 rapamycin in the control of stem cells and their progeny in the drosophila ovary. Development
498 2010, Jul;137(13):2117-26.
499 23. Sun P, Quan Z, Zhang B, Wu T, Xi R. TSC1/2 tumour suppressor complex maintains
500 drosophila germline stem cells by preventing differentiation. Development 2010, Aug
501 1;137(15):2461-9.

502 24. Maines JZ, Stevens LM, Tong X, Stein D. Drosophila dmyc is required for ovary cell growth
503 and endoreplication. Development 2004, Feb;131(4):775-86.
504 25. Wang Y, Riechmann V. The role of the actomyosin cytoskeleton in coordination of tissue
505 growth during drosophila oogenesis. Curr Biol 2007, Aug 7;17(15):1349-55.
506 26. Borreguero-Muñoz N, Fletcher GC, Aguilar-Aragon M, Elbediwy A, Vincent-Mistiaen ZI,
507 Thompson BJ. The hippo pathway integrates pi3k-akt signals with mechanical and polarity cues
508 to control tissue growth. PLoS Biol 2019, Oct;17(10):e3000509.
509 27. Tazuke SI, Schulz C, Gilboa L, Fogarty M, Mahowald AP, Guichet A, et al. A germline-
510 specific gap junction protein required for survival of differentiating early germ cells. Development
511 2002, May;129(10).
512 28. Bohrmann J, Zimmermann J. Gap junctions in the ovary of drosophila melanogaster:
513 Localization of innexins 1, 2, 3 and 4 and evidence for intercellular communication via innexin-2
514 containing channels. BMC Dev Biol 2008;8:111.
515 29. Sahu A, Karmakar S, Halder S, Ghosh G, Acharjee S, Dasgupta P, et al. Germline soma
516 communication mediated by gap junction proteins regulates epithelial morphogenesis. PLoS
517 Genet 2021;17(8).
518 30. Gilboa L, Forbes A, Tazuke SI, Fuller MT, Lehmann R. Germ line stem cell differentiation in
519 drosophila requires gap junctions and proceeds via an intermediate state. Development 2003,
520 Dec;130(26).
521 31. Mukai M, Kato H, Hira S, Nakamura K, Kita H, Kobayashi S. Innexin2 gap junctions in
522 somatic support cells are required for cyst formation and for egg chamber formation in
523 drosophila. Mech Dev 2011, Sep;128(7-10).
524 32. Pesch YY, Dang V, Fairchild MJ, Islam F, Camp D, Kaur P, et al. Gap junctions mediate
525 discrete regulatory steps during fly spermatogenesis. PLoS Genet 2022;18(9).
526 33. Smendziuk CM, Messenberg A, Vogl AW, Tanentzapf G. Bi-directional gap junction-
527 mediated soma-germline communication is essential for spermatogenesis. Development
528 2015;142(15).
529 34. Vachias C, Fritsch C, Pouchin P, Bardot O, Mirouse V. Tight coordination of growth and
530 differentiation between germline and soma provides robustness for drosophila egg
531 development. Cell Rep 2014, Oct 23;9(2):531-41.
532 35. Domanitskaya E, Anllo L, Schüpbach T. Phantom, a cytochrome P450 enzyme essential for
533 ecdysone biosynthesis, plays a critical role in the control of border cell migration in drosophila.
534 Dev Biol 2014;386(2).
535 36. Venken KJ, Schulze KL, Haelterman NA, Pan H, He Y, Evans-Holm M, et al. MiMIC: A highly
536 versatile transposon insertion resource for engineering drosophila melanogaster genes. Nat
537 Methods 2011, Sep;8(9):737-43.
538 37. Isasti-Sanchez J, Münz-Zeise F, Lancino M, Luschnig S. Transient opening of tricellular
539 vertices controls paracellular transport through the follicle epithelium during drosophila
540 oogenesis. Dev Cell 2021;56(8).
541 38. Potter CJ, Tasic B, Russler EV, Liang L, Luo L. The Q system: A repressible binary system
542 for transgene expression, lineage tracing, and mosaic analysis. Cell 2010;141(3).
543 39. Rørth P. Gal4 in the drosophila female germline. Mech Dev 1998, Nov;78(1-2).
544 40. Shimada Y, Burn KM, Niwa R, Cooley L. Reversible response of protein localization and
545 microtubule organization to nutrient stress during drosophila early oogenesis. Dev Biol
546 2011;355(2).
547 41. Riggs CL, Kedersha N, Ivanov P, Anderson P. Mammalian stress granules and P bodies at a
548 glance. J Cell Sci 2020;133(16).
549 42. Cadena Sandoval M., Heberle AM, Rehbein U, Barile C, JM RP, Thedieck K. MTORC1
550 crosstalk with stress granules in aging and age-related diseases. Frontiers in Aging 2021;2.
551 43. Kosakamoto H, Okamoto N, Aikawa H, Sugiura Y, Suematsu M, Niwa R, et al. Sensing of the
552 non-essential amino acid tyrosine governs the response to protein restriction in drosophila. Nat
553 Metab 2022, Jul;4(7).
554 44. Srivastava A, Lu J, Gadalla DS, Hendrich O, Grönke S, Partridge L. The role of GCN2 kinase
555 in mediating the effects of amino acids on longevity and feeding behaviour in drosophila.
556 Frontiers in Aging 2022;3.

557 45. Kang MJ, Vasudevan D, Kang K, Kim K, Park JE, Zhang N, et al. 4E-BP is a target of the
558 GCN2-ATF4 pathway during drosophila development and aging. J Cell Biol 2017;216(1).
559 46. Jewell JL, Russell RC, Guan KL. Amino acid signalling upstream of mtor. Nat Rev Mol Cell
560 Biol 2013, Mar;14(3).
561 47. Carvalho-Santos Z, Cardoso-Figueiredo R, Elias AP, Tastekin I, Baltazar C, Ribeiro C.
562 Cellular metabolic reprogramming controls sugar appetite in drosophila. Nat Metab 2020,
563 Sep;2(9).
564 48. Su YQ, Sugiura K, Eppig JJ. Mouse oocyte control of granulosa cell development and
565 function: Paracrine regulation of cumulus cell metabolism. Semin Reprod Med 2009,
566 Jan;27(1):32-42.
567 49. Rodríguez-Nuevo A, Torres-Sanchez A, Duran JM, De Guirior C, Martínez-Zamora MA, Böke
568 E. Oocytes maintain ros-free mitochondrial metabolism by suppressing complex I. Nature 2022,
569 Jul;607(7920):756-61.
570 50. Cerqueira Campos F, Dennis C, Alégot H, Fritsch C, Isabella A, Pouchin P, et al. Oriented
571 basement membrane fibrils provide a memory for f-actin planar polarization via the dystrophin-
572 dystroglycan complex during tissue elongation. Development 2020;147(7).
573 51. Aigouy B, Umetsu D, Eaton S. Segmentation and quantitative analysis of epithelial tissues.
574 Methods Mol Biol 2016;1478:227-39.
575 52. Aigouy B, Mirouse V. ScientiFig: A tool to build publication-ready scientific figures. Nat
576 Methods 2013, Oct 30;10(11):1048.
577
578

579 **Figure legends**

580

581 **Figure 1: Soma-germline gap junctions are required for germline growth**

582 A) Scheme of an ovariole, oriented from the anterior (A) to the posterior (P) end, as all the
583 subsequent images. The ovariole starts with the germarium from which young follicles bud before
584 undergoing massive growth until the formation of an egg at the posterior end. In each follicle,
585 somatic follicle cells (in purple) surround a germline cyst with the nurse cells (pink) and the oocyte
586 (in blue). B) Sagittal view and C) Maximum intensity projection images of a stage 7 follicle after
587 immunostaining for Inx2 (green in B and C, white in B' and C') and Inx4 (magenta in B and C, white
588 in B'' and C''). D) and E) Higher magnification of the insets in B and C to illustrate the formation of
589 plaques at the germline-soma interface. F) Immunostaining for Inx2 (green in F and F', white in
590 F''') and Inx4 (magenta in F', white in F'') in a follicle containing a *Inx2* RNAi-expressing clone in
591 follicle cells marked by GFP expression (white in F). G) Maximum intensity projection of
592 immunostaining for Inx2 (green in G, white in G'' and G''') and Inx4 (magenta in G, white in G') in
593 follicles containing *Inx4* RNAi-expressing germline clones visualized by Inx4 absence. Note the
594 absence of Inx2 plaques at germline contacts at higher magnification (G''') and the growth defect
595 of *Inx4* RNAi follicles (arrow) compared with the wild-type younger follicle (arrowhead) (G''). H)
596 Somatic $Inx2^{A}$ mutant clones, marked by the absence of RFP expression, induce a germline
597 growth defect when they cover the whole epithelium (arrow) compared with the wild-type younger
598 follicle (n-1) (arrowhead). I) Quantification of the ratio between the volume of the follicle showing a
599 growth defect fully covered by *Inx2* mutant cells, and the volume of the n-1 follicle of the same
600 ovariole (n= 10 control and 7 *Inx2* mutant follicles, Mann-Whitney test). J-K) quantification of J)
601 cell surface and K) EDU-positive cells in small mutant *Inx2* clones compared with the surrounding
602 wild-type cells (n= 20, 20 clones or groups of wild-type cells for J and K, Welch's t test). L)
603 Quantification of the volume ratio between a follicle with *Inx4* RNAi in the germline cyst and the
604 wildtype n-1 follicle of the same ovariole (n= 13 for control and n=17 for *Inx4* RNAi, Mann-Whitney
605 test). For all graphs, data are the mean ± SD. ***p <0.01, ****p <0.0001. Scale bars: 50 μm in B,G,H
606 and 10 μm in E,F.

607

608 **Figure 2: TRAP analysis identifies soma-specific expression of amino acid metabolism and**
609 **transport genes**

610 A) Representative images of follicles expressing RPL10a-GFP in the soma (driven by tj:Gal4) or
611 the germline (driven by nos:Gal4p16). After polysome immunoprecipitation (IP), mRNAs were
612 sequenced. B) The expression of 811 genes was significantly enriched in somatic cells compared
613 with germline cells (fold change >5, p-value <0.05). After filtering for genes involved in small
614 molecule metabolism or transport, genes related to amino acid biology were identified. C)
615 Distribution (soma and/or germline) of genes encoding proteins implicated in amino acid

616 biosynthesis or transport according to their expression profile. No gene of these classes was
617 enriched exclusively in the germline.
618
619 **<u>Figure 3:</u> Amino acid import in follicle cells promotes germline growth**
620 A-B) Representative images of ovaries in A) control and B) after *CG43693* knock-down by RNAi
621 in somatic cells. C) Ovary size (surface) quantification in control and after *CG43693* somatic
622 knock-down using two RNAi lines (Ordinary one-way ANOVA + Dunnett's multiple comparisons
623 test). D-E) In situ hybridization analysis of *CG43693* expression in D) a whole ovariole and in E)
624 stage 4 and 7 follicles. F) Expression of endogenous CG43693 protein tagged with GFP from
625 germarium to stage 8. G) Higher magnification of follicle cells showing CG43693-GFP localization
626 in the cell cortex. H) *CG43693/cochonnet (coch)* mutant clones marked by the absence of RFP.
627 When all somatic cells of a follicle are mutated, follicle growth is affected (arrow) as seen when
628 compared with the younger follicle (arrowhead). I) Quantification of the ratio between the volume
629 of follicle with a growth defect and fully covered by mutant cells and the n-1 follicle in the same
630 ovariole (n= 10 control and 6 *coch* mutant follicles, Mann-Whitney test). J-K) quantification of J)
631 cell surface and K) EDU-positive cells in small *coch* mutant clones compared with the surrounding
632 wild-type cells (n=12 control and 12 mutant clones or groups of wild-type cells, Welch's t test).
633 For all graphs, data are the mean ± SD. **p <0.01, ***p <0.001. Scale bars: 500 μm in A,B, 50 μm
634 D,E,F,H and 10 μm in G.
635
636 **<u>Figure 4:</u> Ectopic amino acid import in the germline compensates its absence in the soma**
637 A) scheme representing *coch* expression in green in the different genotypes used on this figure.
638 B-E) Representative images of a full ovary from B) a control female, C) a *MatTub> coch* female D)
639 a *tj > coch RNAi* female, a *MatTub> coch* female and E) a *tj > coch RNAi*, *MatTub> coch* female.
640 F) Quantification of ovary size (surface) in the indicated genotypes (n = 14, 10, 19, and 27 ovaries,
641 Ordinary one-way ANOVA +Tukey's multiple comparisons test). For all graphs, data are the mean
642 ± SD., ***p <0.001, ****p <0.0001. Scale bars: 500 μm.
643
644 **<u>Figure 5:</u> Defective gap junctions or amino acid import induces P-body formation**
645 A-B) Endogenous GFP-tagged Me31B protein expression in stage 9 follicles in A) well fed
646 conditions or B) after 15 hours of protein starvation. C) P-body quantification in normal and starved
647 conditions. D-E) Me31B-GFP expression in ovarioles germline that overexpresses D) wild-type
648 eIF2α or E) or eIF2α-S51D (inhibitory phosphorylation). F and H) Representative images of Me31B-
649 GFP expression in stage 9 follicles after RNAi-based knock-down in somatic cells of F) *Inx2* or H)
650 *coch*. G and I) P-body quantification in follicles after RNAi-based knock-down in somatic cells of
651 G) *Inx2* and I) *coch.* For all graphs, data are the mean ± SD, ***p <0.001, ****p <0.0001, Unpaired
652 t test. Scale bars: 50 μm.

653

654 **<u>Figure 6:</u> Gap junctions are controlled by the InR/PI3K pathway**

655 A,B) Representative images of Me31B-BFP expression in stage 9 follicles from A) a control female
656 and B) a *tj:Gal4, Tub:Gal80^{ts} > akt RNAi* female. C) P-bodies quantification (fluorescence intensity)
657 in the indicated genotypes (n = 8 and 9 follicles, unpaired t test). Data are the mean ± SD. ****p
658 <0.0001. D) Inx2 expression in an *akt^{q}* mutant clone (marked by the absence of GFP expression).
659 E-F) Inx2 protein (E) and *Inx2* mRNA expression by FISH (F) in a *Pten^{dj189}* mutant clone marked by
660 the absence of RFP expression. G) Large MARCM *Pten^{dj189}* mutant clone marked by the presence
661 of GFP expression showing faster follicle growth. H) Large MARCM *Pten^{dj189}* mutant clone in which
662 faster follicle growth was abolished after expression of an RNAi against *Inx2*. I) Quantification of
663 volume ratio between the older fully wild-type follicle and follicles containing a majority of *Pten*
664 mutant cells and expressing or not RNAi against *Inx2* and (n = 10 and 9, Mann-Whitney test).
665 Scale bars: 50 μm in A, B, G, H and 20 μm in D,E,F. Data are the mean ± SD. ****p <0.0001.

666
667

Figure 1

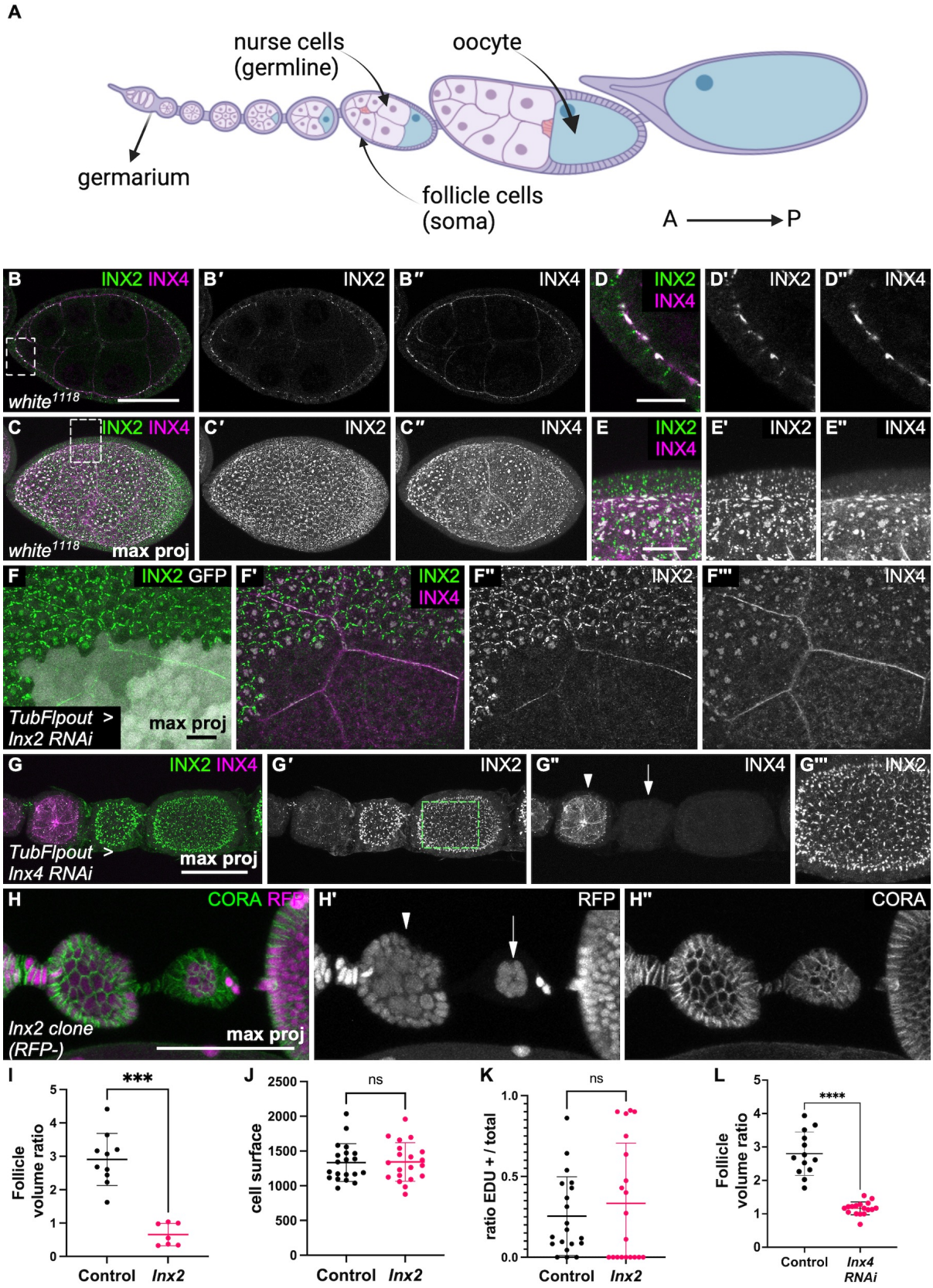
A
nurse cells
(germline)
oocyte
germarium
follicle cells
(soma)
A
P
B
INX2 INX4
white1118
B'
INX2
B''
INX4
D
INX2
INX4
D'
INX2
D''
INX4
C
INX2 INX4
white1118
max proj
C'
INX2
C''
INX4
E
INX2
INX4
E'
INX2
E''
INX4
F
INX2 GFP
TubFlpout >
Inx2 RNAi
max proj
F'
INX2
INX4
F''
INX2
F'''
INX4
G
INX2 INX4
TubFlpout >
Inx4 RNAi
max proj
G'
INX2
G''
INX4
G'''
INX2
H
CORA RFP
Inx2 clone
(RFP-)
max proj
H'
RFP
H''
CORA
I
***
Follicle
volume ratio
Control
Inx2
J
ns
cell surface
Control
Inx2
K
ns
ratio EDU + / total
Control
Inx2
L
****
Follicle
volume ratio
Control
Inx4
RNAi

Figure 2

A

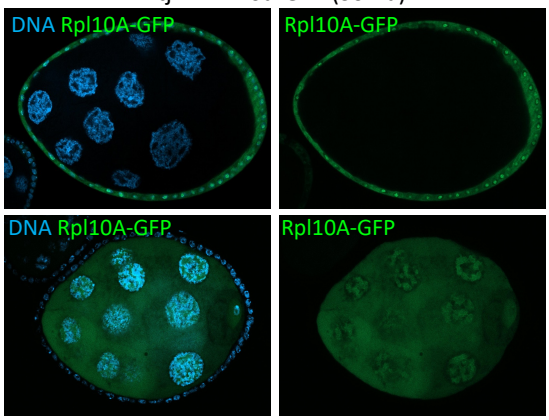

Polysome IP + mRNA Seq

Polysome IP + mRNA Seq

Soma Vs Germline differential expression

B

Soma Vs Germline differential expression	GO Filter	GO analysis	Gene identity
Fold Change >5 *811 genes*	Small molecule metabolic process (GO:0044281) *52 genes (/745)*	Amino acid biosynthesis (GO:0008652) *6 genes (/40)*	*CG10621, CG10623, CG1673, Gs2, GLS, P5CS*
	Transmembrane transporters (GO:0022857) *56 genes (/757)*	Amino acid transporters (GO:0015171) *12 genes (/60)*	*kar, CG15279, CG1628, CG1698, CG16700, NKCC, CG31904, Eaat1, Ncc69, CG43693, CG7888, sbm*

C

Amino acid biosynthesis (GO:008652) *(40 genes)*

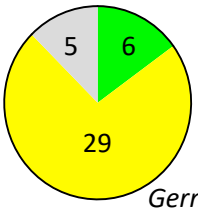

Germline : 0

D

Amino acid transporters (GO:0015171) (*60 genes*)

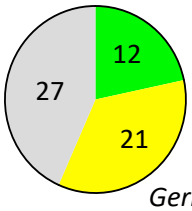

Germline : 0

Soma
Germline
Soma and Germline
not expressed

Figure 3

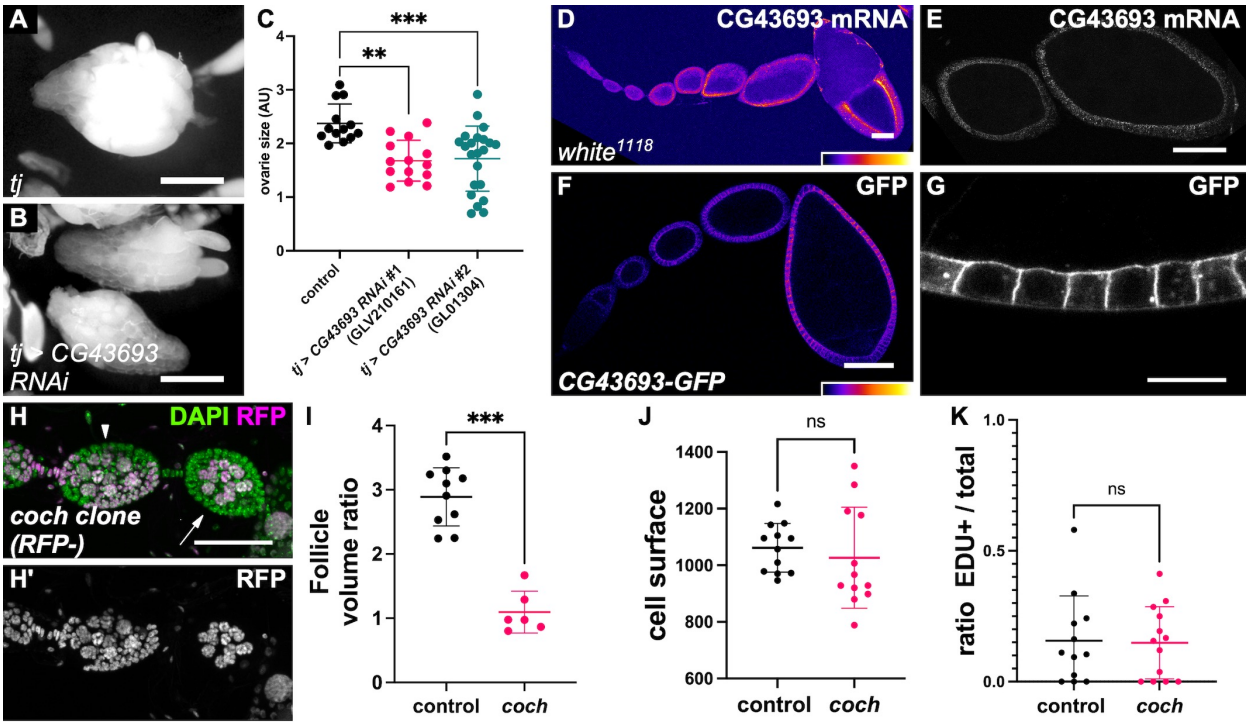
A
tj
B
tj > CG43693 RNAi
C
***
**
ovarie size (AU)
control
tj > CG43693 RNAi #1 (GLV210161)
tj > CG43693 RNAi #2 (GL01304)
D
CG43693 mRNA
white1118
E
CG43693 mRNA
F
GFP
CG43693-GFP
G
GFP
H
DAPI RFP
coch clone (RFP-)
H'
RFP
I
***
Follicle volume ratio
control
coch
J
ns
cell surface
control
coch
K
ns
ratio EDU+ / total
control
coch

Figure 4

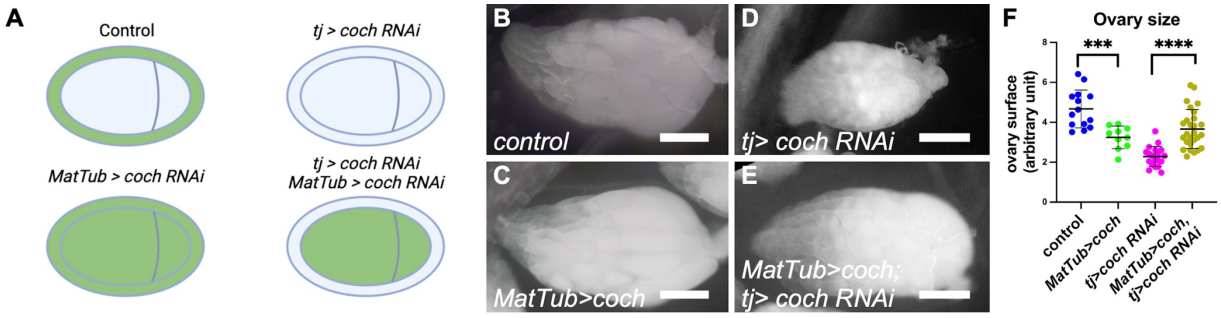
A
Control
tj > coch RNAi
MatTub > coch RNAi
tj > coch RNAi
MatTub > coch RNAi
B
control
D
tj> coch RNAi
C
MatTub>coch
E
MatTub>coch;
tj> coch RNAi
F
Ovary size
***
****
ovary surface
(arbitrary unit)
0
2
4
6
8
control
MatTub>coch
tj>coch RNAi
MatTub>coch,
tj>coch RNAi

Figure 5

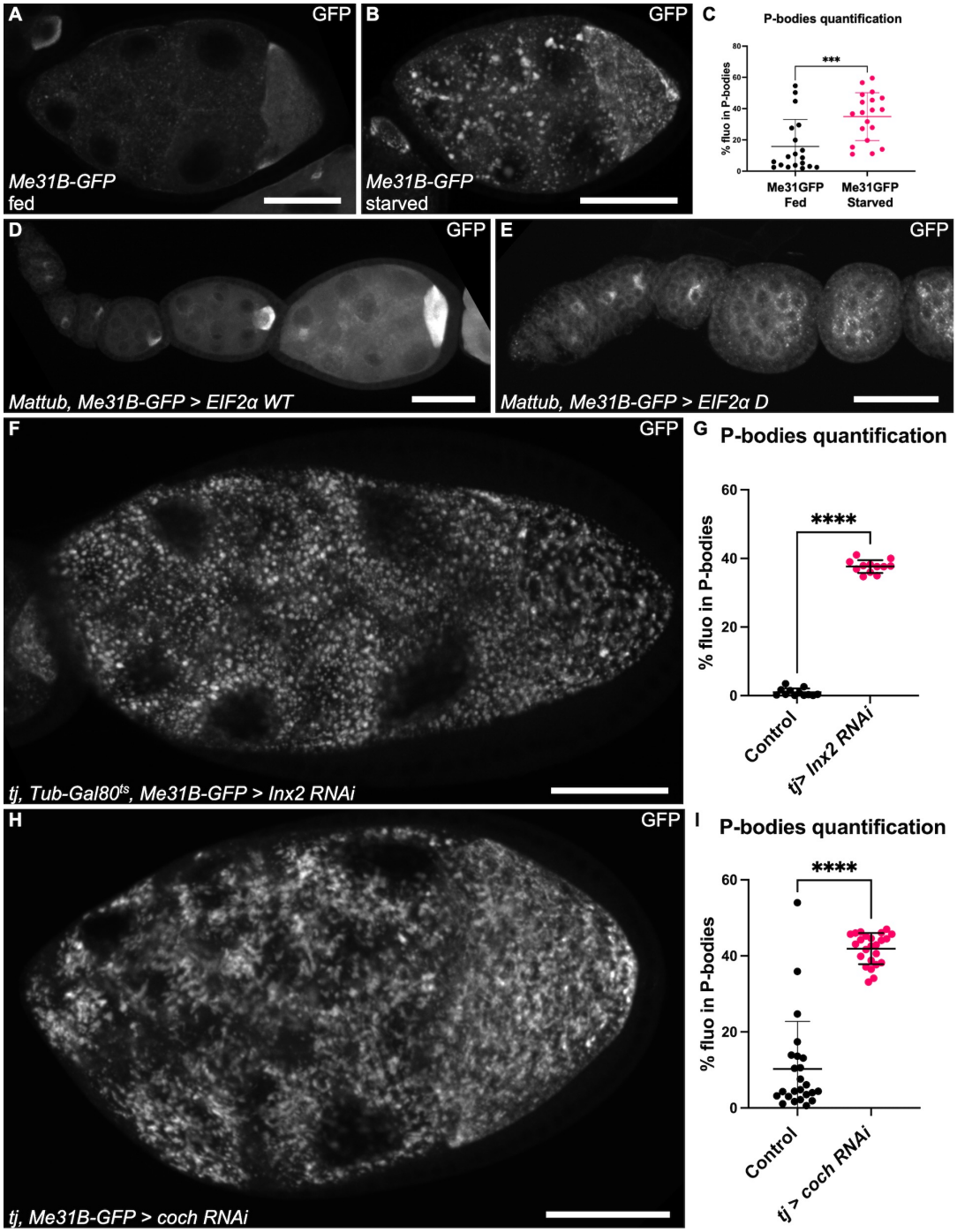
A
GFP
Me31B-GFP
fed
B
GFP
Me31B-GFP
starved
C
P-bodies quantification
% fluo in P-bodies
***
Me31GFP Fed
Me31GFP Starved
D
GFP
Mattub, Me31B-GFP > EIF2α WT
E
GFP
Mattub, Me31B-GFP > EIF2α D
F
GFP
tj, Tub-Gal80ts, Me31B-GFP > Inx2 RNAi
G
P-bodies quantification
% fluo in P-bodies
****
Control
tj> Inx2 RNAi
H
GFP
tj, Me31B-GFP > coch RNAi
I
P-bodies quantification
% fluo in P-bodies
****
Control
tj > coch RNAi

Figure 6

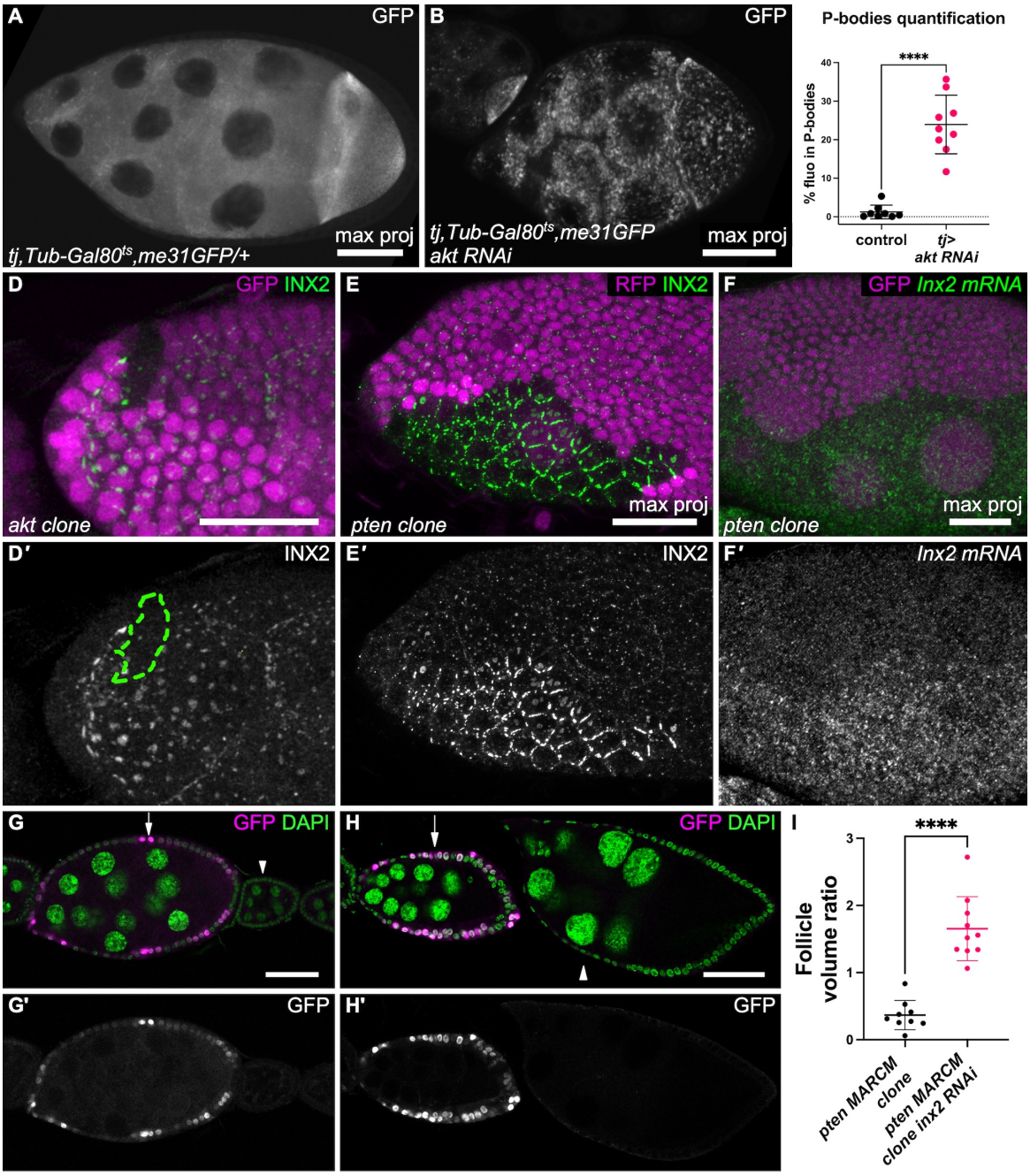
A
GFP
max proj
tj,Tub-Gal80ts,me31GFP/+
B
GFP
max proj
tj,Tub-Gal80ts,me31GFP
akt RNAi
P-bodies quantification
****
% fluo in P-bodies
40
30
20
10
0
control
tj>
akt RNAi
D
GFP INX2
akt clone
E
RFP INX2
max proj
pten clone
F
GFP Inx2 mRNA
max proj
pten clone
D'
INX2
E'
INX2
F'
Inx2 mRNA
G
GFP DAPI
H
GFP DAPI
I
****
Follicle volume ratio
3
2
1
0
pten MARCM clone
pten MARCM clone inx2 RNAi
G'
GFP
H'
GFP

Supplemental data

Supplemental data include :

- 6 supplemental figures
- Table S1 : Excel file of soma vs germline TRAP analysis
- Table S2 : Reagents and resources
- Table S3 : Genotypes and specific conditions

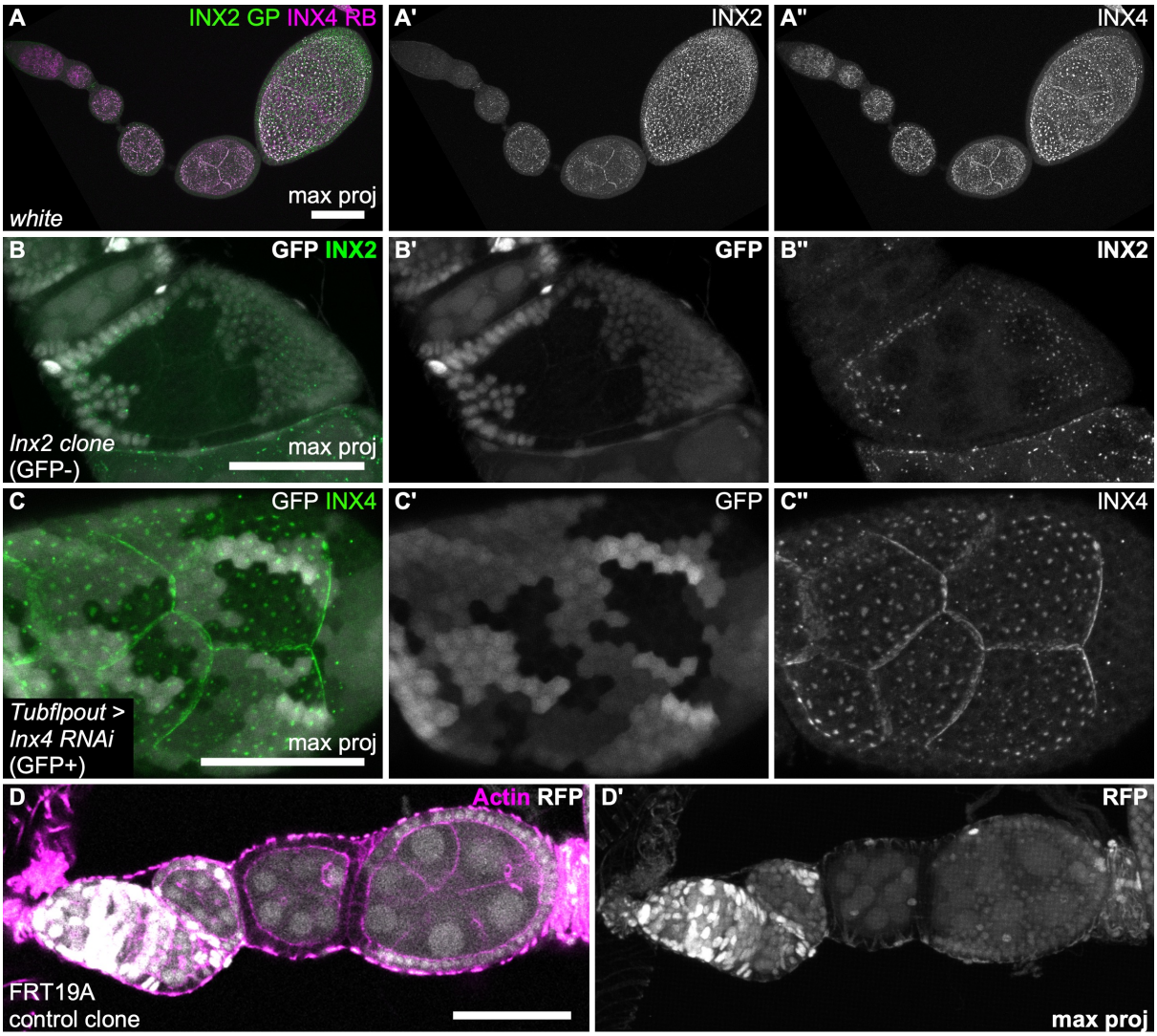

Figure S1

A) Maximum intensity projection images of an ovariole after immunostaining for Inx2 (green in A, white in A') and Inx4 (magenta in A ,white in A"). Note the progressive increase of Inx2 expression. B) follicle containing a germline mutant clone for *Inx2* (absence of GFP white in B and B') and showing no growth defect and no impact on gap junction plaques while Inx2 staining (green in B, white in B")is lost in the somatic clone observed on the same follicle C) Somatic *Inx4* RNAi clone showing no impact on plaque formation (Inx4 staining green in C,white in C"). D) Control FRT19A RFP minus clone covering the whole epithelium of a follicle and showing no growth defect when compared to surrounding follicles. Scale bars 50 μm

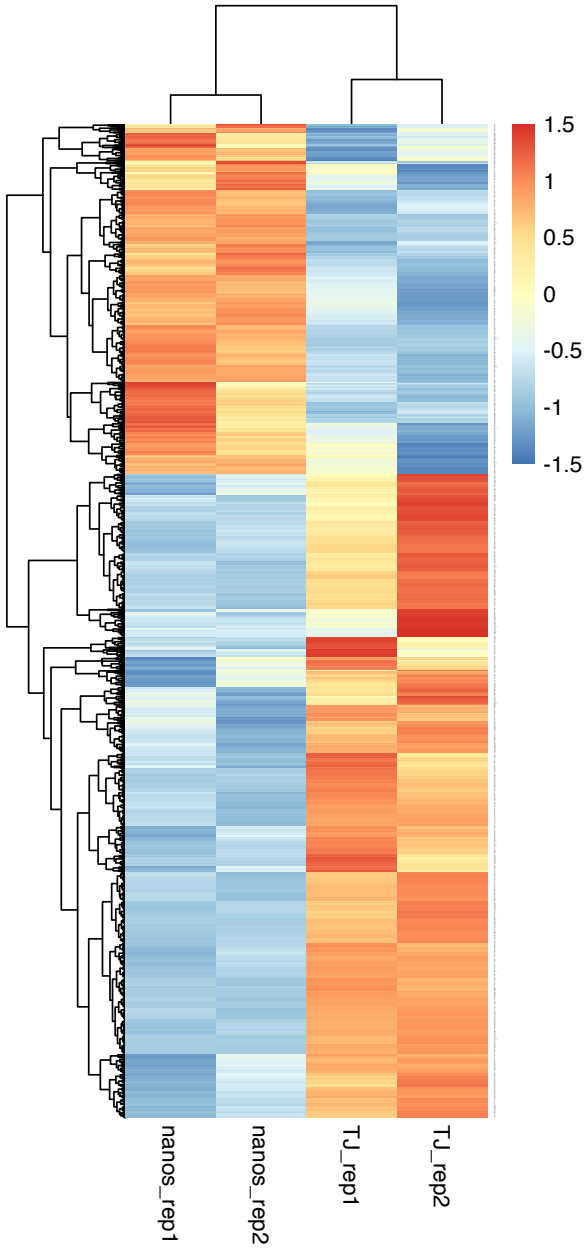

Figure S2

Z-score hierarchical clustering heat map visualization. Only significantly differentially expressed genes are reported. Highly expression correlation can be noticed across condition replicates.

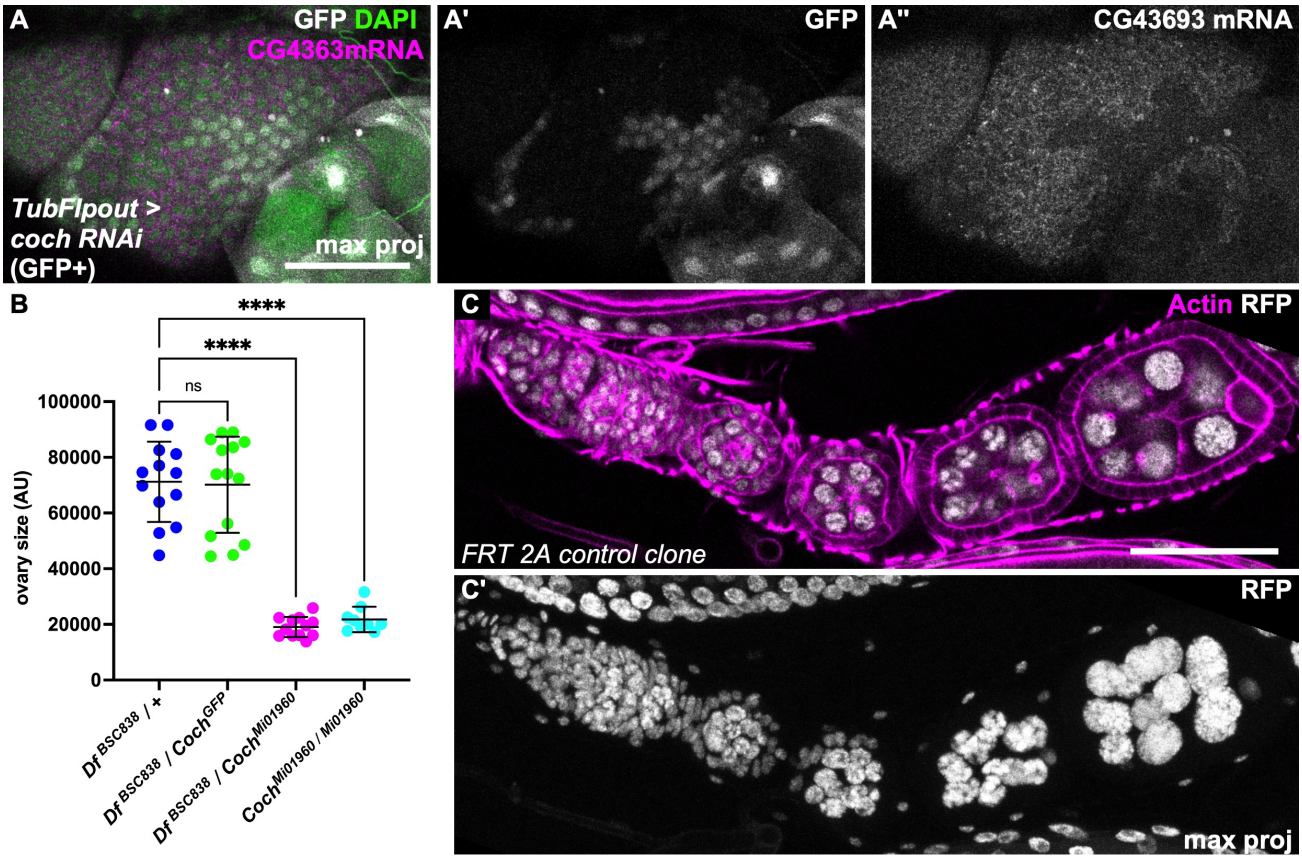

Figure S3

A) RNAi clone against *CG43693/coch* stained by FISH against *CG43693/coch* showing its disappearance from these cells, confirming probe specificity and RNAi efficiency. B) Quantification of ovary size (in arbitrary units) for the indicated genotypes. Data are the mean ± SD. ****p <0.0001. C) Control FRT 2A RFP minus clone covering the whole epithelium of a follicle and showing no growth defect when compared to surrounding follicles. Scale bars 50 μm

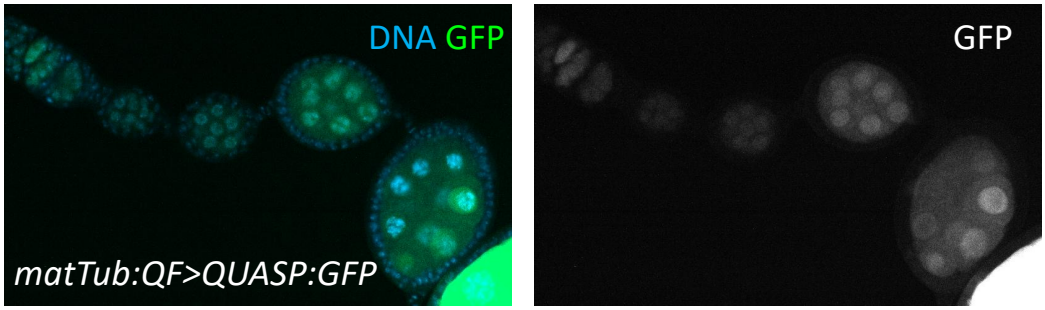

Figure S4
Ovariole expressing a QUASP:GFP transgene under the control of the MatTub:QF driver.

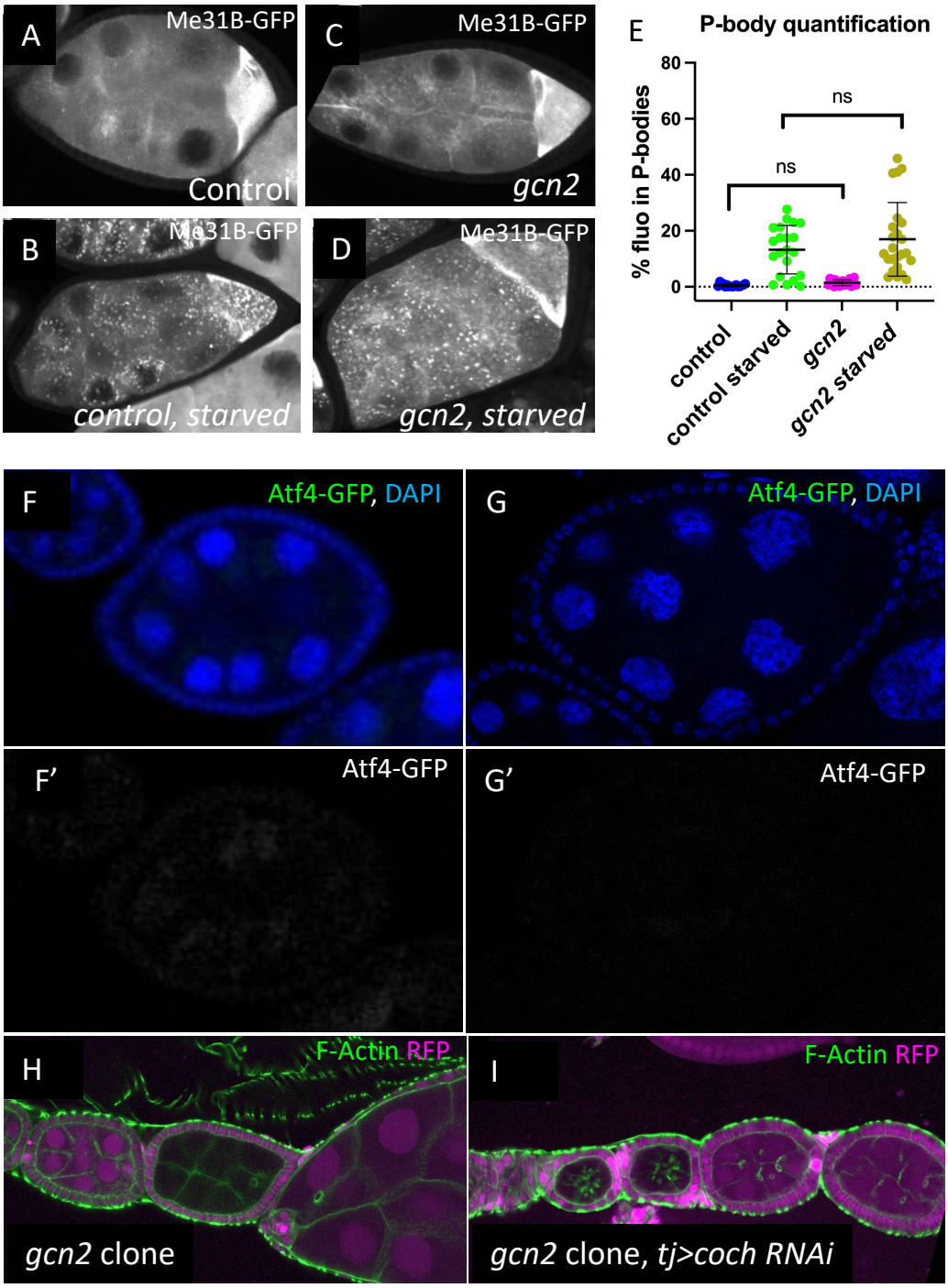

Figure S5

A,B) Representative images of Me31B-BFP expression in stage 9 follicles from a: A) control female, B) starved control female, C) *gcn2* transheterozygous mutant female, and D protein starved *gcn2* transheterozygous mutant female. E) P-bodies quantification (fluorescence intensity) in follicles of the indicated genotypes and conditions. Data are the mean ± SD. F,G) Absence of Atf4-GFP protein expression used as a read-out of GCN2 activity in F) normal and G) protein-starved conditions (green in F and G., white in F' and G'). H-I) Ovarioles with germline *gcn2* mutant clones marked by the absence of RFP expression (magenta) and stained for F-actin (green) in H) wild-type background and I) in flies harbouring *coch* RNAi in follicle cells.

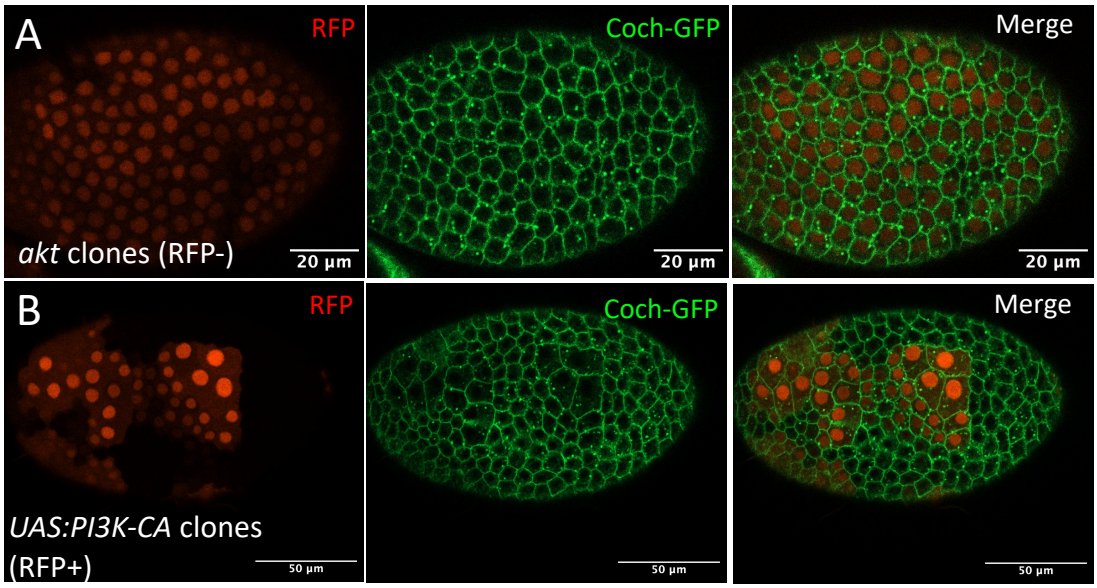

Figure S6

A) Coch-GFP expressing follicle with *akt* mutant clones (RFP-negative cells). B) Coch-GFP expressing follicle with flip-out clones that express a constitutively active form of PI3K (RFP-positive cells).

Table S2: Resources and reagents

RESOURCE OR REAGENT	SOURCE	IDENTIFIER
Experimental models: Organisms/Strains		
tj:Gal4 : P{w+mW.hs=GawB}NP1624	Kyoto Stock Center (DGRC)	FlyBase ID: FBti0034540; DGRC: 104055
FRT19A, Inx2^{A}	Bloomington Drosophila Stock Center	FlyBase ID: FBal0291304; BDSC: 54481
FRT19A, Inx2^{B}	Bloomington Drosophila Stock Center	FlyBase ID: FBal0291305; BDSC: 52363
FRT19A, Inx2^{G0173a}	Bloomington Drosophila Stock Center	FlyBase ID: FBal0151828; DGRC: 111858
UAS :Inx2 RNAi (JF02446)	Bloomington Drosophila Stock Center	FlyBase ID: FBti0128670; BDSC: 29306
UAS : Inx4 RNAi (GL00447)	Bloomington Drosophila Stock Center	FlyBase ID: FBtp0068601; BDSC: 35607
nos:Gal4Vp16	Bloomington Drosophila Stock Center	FlyBase ID: FBti0012410; BDSC: 4937
MatTub :Gal4Vp16 (V2H)	Bloomington Drosophila Stock Center	FlyBase ID: FBti0016915; BDSC: 7062
UASp-RPL10a-GFP	Junion G.	Nd
UAS : CG43693 RNAi (GLV21061)	Bloomington Drosophila Stock Center	FlyBase ID: FBti0144657; BDSC: 35696
UAS : CG43693 RNAi (GL01304)	Bloomington Drosophila Stock Center	FlyBase ID: FBti0149385; BDSC: 41873
CG43693/Coch ^{MI01960} : Mi{MIC}CG43693^{MI01960}	Bloomington Drosophila Stock Center	FlyBase ID: FBti0132690; BDSC: 34264

Coch/CG43693-EGFP : CG43693 MI01960-GFSTF.0	This study	
DF(3L)BSC838	Bloomington Drosophila Stock Center	FlyBase ID: FBab0046056 BDSC: 29023
Me31B-GFP : P{PTT-GB}me31B^{CB05282}	Bloomington Drosophila Stock Center	FlyBase ID: FBal0211797 BDSC: 51530
UASz : eIF2a	This study	
UASz : eIF2a-S51A	This study	
UASz : eIF2a-S51D	This study	
MatTub :QF	This study	
QUASp :EGFP	This study	
QUASp :Coch	This study	
UAS :gcn2 sgRNA	Vienna Drosophila Resource Center	VDRC: 341108
nos:Gal4Vp16, ; UAS:Cas9	Bloomington Drosophila Stock Center	BDSC: 54593
FRT gnc2^{CB20}	This study, contains a 2n postion 878 (gg) on gcn2-RA transcript	
FRT gcn2^{CB14}	This study, contains a 1n deletion at position 877 (a) and a 9n insertion (tttccgacc) on gcn2-RA transcript	
4E-BPintron-dsRed	Kang et al, J Cell Biol, 2017	FlyBase ID: FBtp0116205
ATF4-GFP : Mi{PT-GFSTF.1}crcMI02300-GFSTF.1	Bloomington Drosophila Stock Center	FlyBase ID: FBal0314614; BDSC: 59608
FRT40A, Pten^{dj189}	Pan D.	FlyBase ID: FBal0117670
FRT82B, akt^{q}	S. Cohen	Nd
UAS : akt RNAi (HM04007)	Bloomington Drosophila Stock Center	FlyBase ID: FBti0130466 BDSC 31701
UAS : PI3K-CA (Chromosome II)	This study, obtained by P-element mobilization	

	of UAS:PI3K92E-CAAX (FBal0156077)	
Antibodies		
anti-Inx4, rabbit	G. Tanentzapf	1/2000
anti-Inx2, Guinea Pig	G. Tanentzapf	1/400
anti-Inx2 rabbit	P. Phelan	1/5000
anti-coracle mouse	DSHB	C615.16 1/100
anti-mouse –Alexa 488	Life technologies	A21202 1/1000
anti-rabbit -Cy5, Donkey	Jackson Immunoresearch	711-175-152 dilution 1/1000
Anti-rabbit pig-Cy3, Donkey	Jackson Immunoresearch	711-165-152 dilution 1/1000
anti-guinea pig-Cy5, Donkey	Jackson Immunoresearch	703-175-155; dilution 1/1000
Anti-guinea pig-Cy3, Donkey	Jackson Immunoresearch	706-165-148 dilution 1/1000
Chemicals, Peptides, kits		
Phalloidin Atto-488, -550, -633	Sigma	#49409, #19083, #68825
DAPI	Sigma	100 µg/ml D8417-1MG
EdU Click-iT™ Plus Alexa 555	Thermo Fisher	C10638
Ovation 1-16 droso Universal RNA-seq kit	Nugen	No longer distributed
Software and Algorithms		
Fiji	(Schindelin et al, 2012)	
Prism		

Table S3: Genotypes and specific conditions

(h: hours; HS: heat-shock, GP : grape juice agar plate)

Figure		Genotype	Condition
Figure 1	BE	*w^{1118}*	25°C
	F	*y,w,hs:flp122; Act5C:FRT-Stop-FRT-Gal4, UAS:GFP , UAS:Inx2 RNAi*	1HS, 4 days at 30°C
	G,L	*y,w,hs:flp122; Act5C:FRT-Stop-FRT-Gal4, UAS:GFP , UAS:Inx4 RNAi*	1HS, 4 days at 30°C
	H,J	*FRT19A, Inx2 / FRT19A, Ubi:nlsRFP, hs:flp122*	1HS, 10-12 days at 25°C
	K,L	*FRT19A, Inx2 / FRT19A, Ubi:nlsRFP, hs:flp122*	1HS, 2 days at 25°C
Figure 2	A	*tj:Gal4 / UASp :Rpl10a-GFP and UASp :Rpl10a-GFP; nos:Gal4VP16*	25°C
Figure 3	A	*tj:Gal4*	4 days at 30°C
	B	*tj:gal4 / UAS: CG43693 RNAi ^{GL01304}*	4 days at 30°C
	C	*tj:Gal4*	4 days at 30°C
		tj:gal4 / UAS: CG43693 RNAi^{GLV210161}	
		tj:gal4 / UAS: CG43693 RNAi^{GL01304}	
	D,E	*w^{1118}*	25°C
	F,G	*CG43693-GFP (or coch-GFP)*	25°C
	H,I	*y,w,hs:flp122; FRT2A, coch^{MI01960}/ FRT2A, Ubi:nlsRFP*	2HS, 8 days at 25°C
	J,K	*y,w,hs:flp122; FRT2A, coch^{MI01960}/ FRT2A, Ubi:nlsRFP*	1HS, 2 days at 25°C
Figure 4	A,B,F	*tj:gal4, MatTub:QF, / +*	4 days at 30°C
	A,C,F	*tj:gal4, MatTub:QF,; QUASP:coch*	
	A,D,F	*tj:gal4, MatTub:QF,; UAS: coch RNAi^{GLV21061}*	
	A,E,F	*tj:gal4, MatTub:QF, QUASP:coch; UAS: coch RNAi^{GLV21061}*	
Figure 5	A,C	*Me31B-GFP*	25°C
	B	*Me31B-GFP*	25°C, 14h on GP
	D	*MatTub :Gal4Vp16, Me31B-GFP , UASz: eIF2α*	25°C
	E	*MatTub :Gal4Vp16, Me31B-GFP, UASz: eIF2α-S51D*	25°C
	F,G	*tj:gal4,Tub:Gal80^{ts},Me31B-GFP / UAS:Inx2RNAi*	18°C, 14h at 30°C
	H,I	*tj:gal4, Me31B-GFP / UAS: coch RNAi^{GLV21061}*	2 days at 25 °C
Figure 6	A,C	*tj:Gal4, Tub:Gal80^{ts} Me31B-GFP*	2 days at 30°C
	B,C	*tj:Gal4, Tub:Gal80^{ts,} Me31B-GFP / UAS: akt RNAi*	2 days at 30°C
	D	*y,w,hs:flp122; FRT82B, akt^{q} / FRT82B, Ubi:GFP*	1HS, 4 days at 25°C
	E,F	*y,w,hs:flp122 ; FRT40A,Pten^{dj189} / FRT40A, Ubi:nlsRFP*	1HS, 4 days at 25°C
		y,w,hs:flp122, Tub:Gal4, UAS :GFP ; FRT40A,Pten^{dj189} /	1HS, 5 days at 25°C
	G	*FRT40A, Tub :Gal80*	1HS, 6 days at 25°C

	H	*y,w,hs:flp122, Tub:Gal4, UAS :GFP ; FRT40A,Pten^{dj189} / FRT40A, Tub :Gal80; UAS :Inx2 RNAi*	1HS, 6 days at 25°C
Figure S1	A	*w^{1118}*	25°C
	B	*FRT19A, Inx2 / FRT19A, Ubi:nlsRFP, hs:flp122*	1HS, 5 days at 25°C
	C	*y,w,hs:flp122; Act5C:FRT-Stop-FRT-Gal4, UAS:GFP , UAS:Inx4 RNAi*	
	D	*FRT19A, Ubi:nlsRFP, hs:flp122 / FRT19A, Ubi:GFP*	1HS, 5 days at 25°C
Figure S3	A	*y,w,hs:flp122; Act5C:FRT-Stop-FRT-Gal4, UAS:GFP / UAS: coch RNAi*	1HS, 3 days at 30°C
	B	*DF(3L)BSC838/+* *DF(3L)BSC838 / coch^{MI01960}* *coch^{MI01960} / coch^{MI01960}* *DF(3L)BSC838 / coch-GFP*	25°C
	C	*,w,hs:flp122; FRT2A, coch^{MI01960}/ FRT2A, Ubi:nlsRFP*	1HS, 5 days at 25°C
Figure S4		*MatTub:QF / QUASP:GFP*	25°C
Figure S5	A,C	*Me31B-GFP*	25°C
	B,C	*Me31B-GFP, gcn2^{CB20}/ gcn2^{CB14}*	25°C
	D,E	*ATF4-GFP*	25°C
	H	*y,w,hs:flp122 ; FRT82B, gcn2^{CB14} / FRT82B, Ubi:nlsRFP*	1HS, 5 days at 30°C
	I	*y,w,hs:flp122 ; tj :Gal4 ; UAS: coch RNAi^{GL01304}, FRT82B, gcn2^{CB14} / FRT82B RFP*	1HS, 5 days at 30°C
Figure S6	A	*y,w,hs:flp122 ; coch-GFP, FRT82B, akt^{q} / FRT82B, Ubi:nlsRFP*	1HS, 5 days at 25°C
	B	*y,w, hsflp122; Act5C:FRT-STOP-FRTGal4; UAS:RFP/ UAS:PI3K-CAAX ; coch-GFP*	1HS, 5 days at 25°C